

## PHASE TRANSFORMATIONS AND PHASE DIAGRAM AT EQUILIBRIUM IN THE Cu–Ni–Sn SYSTEM

F. Sadi\* and C. Servant

Laboratoire de Physico-Chimie de l'Etat Solide, ICMMO, UMR CNRS 8182, Bât. 414, Université de Paris-Sud 91405 Orsay Cedex, France

The Cu–Ni–Sn ternary phase diagram in the Cu rich side has not been experimentally determined or calculated at low temperatures. Two Cu<sub>9</sub>Ni<sub>x</sub>Sn alloys with  $x=2$  and 6 mass% Sn were studied. The precipitation sequence during the ageing and phases responsible for the strengthening were determined.

**Keywords:** Calphad method, Cu–Ni–Sn alloys, phase diagrams, phase transformations

### Introduction

The base Cu alloys of the Cu–Ni–Sn ternary system have interesting mechanical and electric properties (the objectives are: tensile strength  $\sim 1000$  MPa,  $\varepsilon$  maximal elongation  $>12\%$  and  $\sigma_e$  electrical conductivity  $>20\%$  IACS) for industrial applications in the electric, electronic (lead frame and connectors), automobile and aeronautical fields. These alloys are potential candidates to replace the Cu alloys with Be addition on account of the Be toxicity for the humanity and environment. The aim of the present work was finally the best assessment of the Cu–Ni–Sn phase diagram at low temperatures. Indeed, this phase diagram is not very well known because it has been experimentally poorly studied in the literature [1]. So, in two Cu–Ni–Sn alloys, we identified the phases formed

and the transformation sequence during ageing which gives rise to remarkable mechanical properties.

### Experimental

The chemical compositions of the studied alloys were measured with the Castaing electron microprobe analysis. They are reported in Table 1.

The studied alloys are industrial ones prepared by continuous casting in 19 mm thick bands. The as-cast material presents a dendritic microsegregation (Fig. 1a) composed of  $\alpha$  dendrites and  $\gamma$  segregation. The dendrites are formed of  $\alpha$ -phase enriched in Cu and depleted in Sn. The interdendritic spaces contain the  $\gamma$ -D0<sub>3</sub>-(Cu, Ni)<sub>3</sub>Sn phase enriched in Sn (Fig. 1b). In order to obtain a reference state, the alloys were homogenized

**Table 1** Chemical compositions of the studied alloys

Designation	Nominal composition/mass%			Analyzed composition/mass%			
	Cu	Ni	Sn	Cu	Ni	Sn	P
A1	90	9	2	balance	9.52	2.42	0.07
A2	85	9	6	“	9.52	5.92	0.06

**Table 2** Symbols and crystal structures of the solid phases in A1 and A1 alloys

Diagram symbol	Composition mass% Sn	Cell parameters/Å this work	Pearson symbol [2]	Space group	Structure designation	Prototype
( $\alpha$ )		3.615	cf4	Fm $\bar{3}$ m	A1	Cu
( $\alpha$ 1)	(Cu–Ni) Depleted in Sn	3.611	cf4	Fm $\bar{3}$ m	A1	Cu
( $\alpha$ 2)	(Cu–Ni) Enriched in Sn	3.641	cf4	Fm $\bar{3}$ m	A1	Cu
D0 <sub>22</sub>		$a=3.77$ $c=7.24$	tI8	I4/mmm	D0 <sub>22</sub>	Al <sub>3</sub> Ti
$\gamma$	34 to 40 in Cu <sub>9</sub> Ni <sub>x</sub> Sn	5.945	cF16	Fm $\bar{3}$ m	D03	BiF <sub>3</sub>

\* Author for correspondence: sadi.faycal@neuf.fr

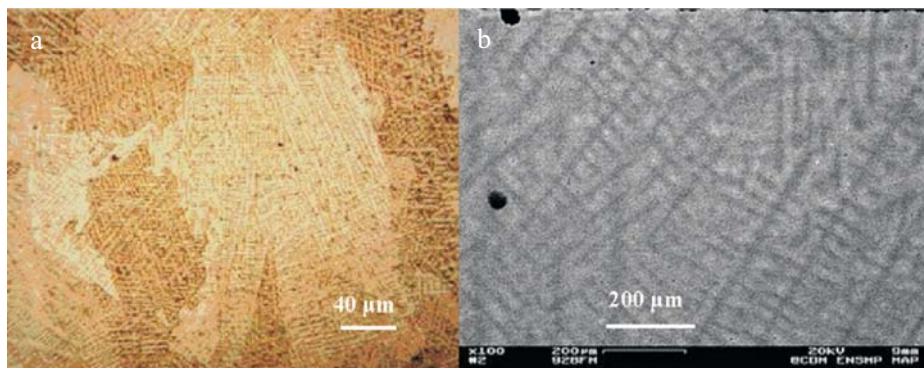


**Fig. 1** a – Optical micrograph of as-cast alloy showing dendritic segregation, b –  $\alpha$ -FCC dendrites and  $\gamma$ -(Cu,Ni)<sub>3</sub>Sn segregation (SEM, back-scattered electrons)

at 820°C for 2 h under neutral N<sub>2</sub> atmosphere, and then water quenched in order to have a grain size of about 100 microns. After homogenization, the lattice parameter of the  $\alpha$ -Cu phase saturated in Sn is equal to  $a=3.641\pm0.001$  Å (Table 2).

After homogenization in the  $\alpha$ -Cu single field, the alloys were cold-rolled with a reduction of 100%, and then they were recrystallized at 780°C during 6 min for the A1 alloy and 4 min for the A2 alloy. The grain size was comprised between 7 and 15 microns. The recrystallized alloys were then aged at 400°C during time comprised between 5 min and 24 h.

The microstructure of the alloys was examined by optical (OM), scanning electron (SEM), transmission electron (TEM) microscopies and X-ray diffraction. The thermal analysis was performed with differential scanning calorimetry (DSC) using a SETARAM device. The tensile tests were carried out on flat samples with the help of an INSTRON type tensile machine. The elongations were measured with an extensometer.

The phase diagrams at equilibrium were determined using the Calphad method [3] and by referring to the thermodatabase previously optimized by Miettinen [1] with the Parrot module of the Thermocalc software [4] at the high temperatures.

## Results and discussion

Figure 2 shows the DSC curves recorded on the A1 and A2 alloys during the cooling from the liquid state with a 40°C min<sup>-1</sup> rate. The temperatures of transformations

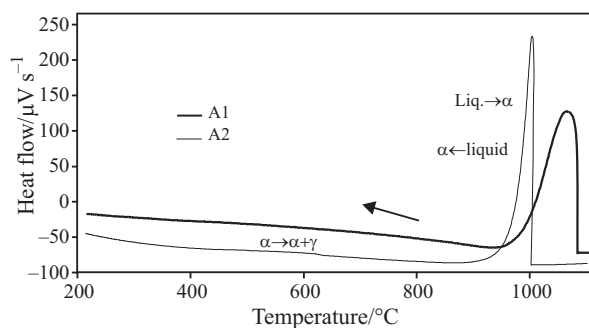


**Fig. 2** DSC analysis showing: liquid $\rightarrow\alpha$  and  $\alpha\rightarrow\alpha+\gamma$  transformations of A1 and A2 alloys during cooling

of the alloys as a function of the Sn content and for cooling rates comprised between 40 and 10°C min<sup>-1</sup> are shown in Table 3. Lower is the Sn content, higher are the temperatures of transformations and specially those of the beginning and end of solidification.

The amount of the precipitated  $\gamma$ -D03-(Cu, Ni)<sub>3</sub>Sn phase is so low that it is not detected by DSC.

### Influence of aging on the mechanical properties

The variations of the maximum tensile strength (Rm), the elasticity limit ( $\sigma_{0.2}$ ) and the tensile elongation are respectively shown in Figs 3a and b for the alloys A1 and A2 vs. the aging time at 400°C. These curves suggest that when the ageing time is increasing, the maximum tensile stress and the elasticity limit also increase while the ductility is decreasing. These phenomena reverse above a certain aging time.

**Table 3** DSC temperatures of transformation during the cooling as a function of Sn content and cooling rate

Alloy	Cooling rate R <sub>c</sub> /°C min <sup>-1</sup>	Temperature of beginning of solidification/°C	Onset of the DSC peak/°C	Temperature of end of solidification/°C	Temperature of transformation $\alpha\rightarrow\gamma$ /°C
A1	40	1084	1064	984	?
	10	1104	1099	1037	?
A2	40	1002	1004	967	578
	10	1061	1056	1045	630

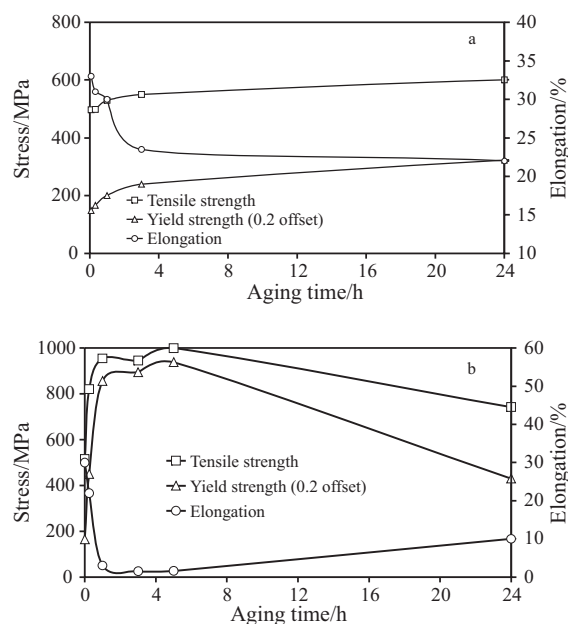


**Fig. 3** Effect of aging time on tensile strength, yield strength and tensile elongation after ageing at 400°C, a – A1 alloy, b – A2 alloy

For the A1 alloy, two regimes seem to govern the mechanical characteristics, (Fig. 3a). When the aging time is lower than 3 h, on the one hand the increase of the tensile strength as well as of the yield strength and on the other hand the decrease of the tensile elongation occurs rapidly. Above this duration, the same phenomenon continues but more slowly and with a quasi-linear evolution.

For the A2 alloy, two regimes of strengthening are observed, (Fig. 3b): a first peak is associated with the strengthening after 15 min, followed by a second peak after 5 h of ageing and then a decrease in ductility. Above this duration, a decrease in the mechanical strengths accompanied by a notable amelioration of the ductility is observed.

The incubation time before the starting of the spinodal decomposition and the D0<sub>22</sub> phase precipitation depends on the chemical composition of alloy considered and especially on the Sn/Ni ratio [5, 6].

It will be noted that the grain size does not change during the ageing.

#### Interpretation of aging microstructure

The increase of mechanical resistance with decrease of ductility in the first steps of the ageing is due to the spinodal decomposition of the alloys [7]. The (FCC)  $\alpha$ -Cu phase decomposes into two phases having the same crystalline structure, the one is Sn enriched, and the other is Sn depleted. An enlargement of the X-ray diffraction peaks gives account of this fact.

The second ageing peak is associated with the formation of the  $\gamma$ -D0<sub>22</sub> phase having (Cu, Ni)<sub>3</sub>Sn chemical composition. This phase is coherent with the  $\alpha$ -Cu matrix, and has a tetragonal symmetry. It has been identified by X-ray diffraction and TEM in the two A1 and A2 alloys. Its lattice parameters are  $a=3.77\pm0.01$  Å and  $c=7.24\pm0.01$  Å.

The image shown in Fig. 4 is a bright field micrograph obtained on the D022 phase formed in the A1 alloy aged for 5 h at 400°C. An important density of coherent particles of the D022 phase having a butterfly wing dark contrast is uniformly scattered in the grain. The size of the particles varies between 8 and 11 nm. In addition, the precipitation of the  $\gamma$ -D0<sub>3</sub> phase is observed as elongated ellipsoidal particles along the grain boundaries. The orientation relationships between the  $\alpha$ -Cu matrix and the D022 phase determined by Baburaj [8] and confirmed in the present work are as follows:

$$(111)_{\alpha\text{-Cu}}//(112)_{\text{D}022} \text{ and } [1\bar{2}1]_{\alpha\text{-Cu}}//[\bar{1}\bar{1}\bar{1}]_{\text{D}022}$$

The diminution of the mechanical strengths accompanied with an increase of the ductility in the case of the A2 alloy have been attributed to the discontinuous precipitation of the  $\gamma$ -(Cu, Ni)<sub>3</sub>Sn phase incoherent with

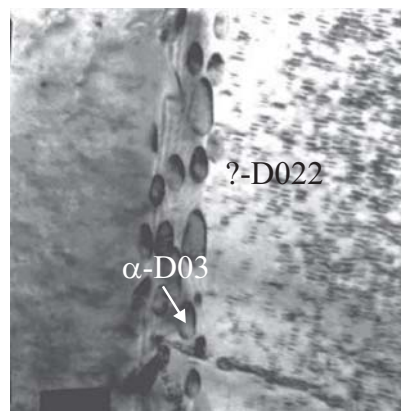


**Fig. 4** TEM bright field images showing the grain boundary  $\gamma$ -D0<sub>3</sub> precipitates and D022 precipitation in  $\alpha$ -Cu matrix (alloy A1, 3 h at 400°C)

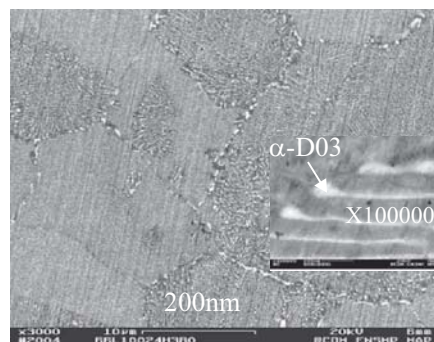


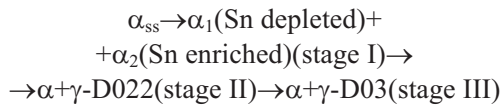
**Fig. 5** Typical discontinuous precipitation  $\alpha+\gamma$ -D03 (alloy A2, 24 h at 400°C). SEM-Back scattered electron micrograph

the matrix (Fig. 5). Its lattice parameter is equal to  $a=5.945\pm0.001$  Å while the one of the  $\alpha$ -Cu matrix ( $a=3.611\pm0.001$  Å) diminishes due to its Sn depletion because of the precipitation of the  $\gamma$ -D03 phase. This latter parameter is practically identical to the one of pure copper. This fact gives account of the total precipitation of Sn, previously dissolved in the matrix, as lamellae of stable  $\gamma$ -D03-(Cu, Ni)<sub>3</sub>Sn phase. The orientation relationships between the two phases are as follows:

$$(111)_{\alpha\text{-Cu}}//(011)_{\text{D}03} \text{ and } [\bar{1}01]_{\alpha\text{-Cu}}//[\bar{1}\bar{1}1]_{\text{D}03}$$

#### Aging model

The microstructural behavior of the studied alloys during aging can be described as the following precipitation sequence:



#### Stage (I)

The strengthening first peak is attributed to the spinodal decomposition. The spinodal strengthening value  $\Delta\tau$  is given by:

$\Delta\tau=(1/6)^{1/2} A \eta Y$  (where  $A$  amplitude of the spinodal modulation,  $\eta=1/a\partial a/\partial c$  the differential size misfit,  $Y=\frac{(C_{11}+2C_{12})(C_{11}-C_{12})}{C_{11}}$  proper elastic constant for Cu-Ni with modulations of Sn along <100> direction).

#### Stage (II)

The strengthening second peak is attributed to the precipitation of the  $\gamma$ -D022 metastable phase. The  $\Delta\tau$  strengthening value is given by:

$$\Delta\tau=3.7\mu_{\text{ef}}\varepsilon^{4/3}f^{2/3}(\rho/b)^{1/3} [9] \text{ (where } \varepsilon=\left|\frac{a_p-a_M}{a_M}\right|$$

misfit,  $f$  final volume fraction of  $\gamma$ -(Cu, Ni)<sub>3</sub>Sn,  $\rho$  diameter of the particles,  $b$  the Burgers vector).

#### Stage (III)

The lost of strengths and the increase in ductility are linked to the discontinuous precipitation (lamellar microstructure of growth of the equilibrium  $\gamma$ -D03 phase from the grain boundaries). Furthermore, it can be noted that the stage (III) is not observed in the case of the A1 alloy, which has a low Sn content. In this alloy, the transformations take place more slowly and the intensity of the phenomena is very much less intense.

#### At equilibrium

Two Cu-9Ni-xSn isopleth sections respectively experimental and calculated are shown in Fig. 6. Contrarily to the prediction of previous experiments by [10], Fig. 6a, and according to our thermodynamic

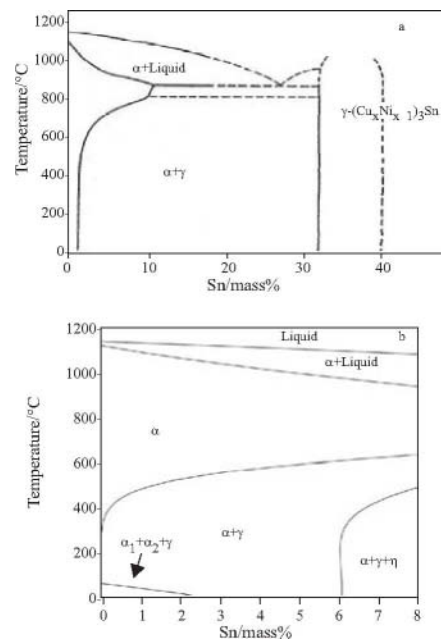


Fig. 6 Cu9Ni-xSn isopleths determined,  
a – experimentally [10] and b – by thermodynamic  
calculation (this work)

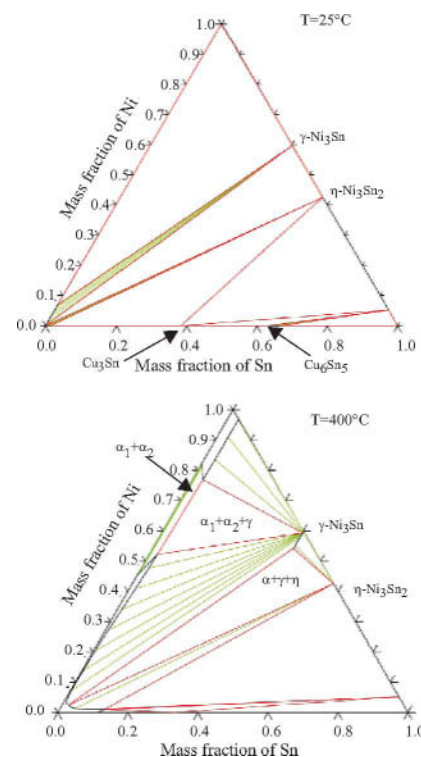


Fig. 7 Isothermal sections calculated at 25 and 400°C

calculation, Fig. 6b, the Sn solubility in the Cu–9Ni alloy is practically equal to 0 at low temperatures. Furthermore, the  $\alpha_1$  and  $\alpha_2$  phases issued from the spinodal decomposition are stable at the room temperature, (Figs 6b and 7a) in the  $(\alpha_1 + \alpha_2 + \gamma)$  ternary domain.

Figures 7a and b represent the isothermal sections calculated respectively at 25 and 400°C.

## Conclusions

We have determined the precipitation sequence of two cupronickel alloys with Sn during the ageing as well as the phases, which are responsible for the strengthening. However, the discontinuous precipitation is not observed in the case of the alloy having a Sn lower content for the performed ageing durations. Due to its mechanical properties, the A2 alloy is the ideal replacing for the cupro-beryllium alloys.

The kinetics of precipitation seems to be governed by the ratio of the Sn/Ni chemical content in the alloys of the Cu–Ni–Sn system.

In addition, by the thermodynamic calculation, isothermal sections at low temperatures (400 and 25°C) have been determined and a Cu<sub>9</sub>Ni<sub>x</sub>Sn new isopleth section has been proposed. On the isothermal section calculated at 400°C, in the rich Cu side, only the  $\alpha$  phase is observed for the compositions studied in the present work; but a two-phase domain ( $\alpha_1 + \alpha_2$ ) is calculated for higher Ni content as in the Cu–Ni

binary system. On the isothermal section calculated at 25°C, this two-phase domain extends over the whole Ni content as in the Cu–Ni binary system.

Further experiments, in particular for higher Sn content, will be needed in order to re-optimize the thermodynamic database used in the present work.

## References

- 1 J. Miettinen, Thermodynamic description of the Cu–Ni–Sn system at the Cu–Ni side, Computer Coupling of Phase Diagrams and Thermochemistry, 27 (2003) 309.
- 2 W. B. Pearson, A handbook of Lattice Spacings and Structure of Metals and Alloys, Pergamon Press, New-York, (1958).
- 3 L. Kaufman and H. Berstein, Computer Calculations of Phase Diagrams, Academic Press, New-York, N.Y., (1970).
- 4 B. Sundman, A. Jansson and J.-O. Andersson, CALPHAD, 9 (1985) 153.
- 5 J. C. Zhao and M. R. Notis, Scripta Met., 39 (1998) 1509.
- 6 J. C. Zhao and M. R. Notis, Acta Mater., 46 (1998) 4203.
- 7 J. W. Cahn, Acta Metall., 11 (1963) 1275.
- 8 E. G. Baburaj, U. D. Kulkarni, E. S. K. Menon and R. Krishnan, J. Appl. Cryst., 12 (1979) 476.
- 9 P. Kratochvil, J. Mencl, J. Pesicka and S. Komnik, Acta Metall., 32 (1984) 1493.
- 10 J. T. Plewes, Metall. Trans., 6A (1975) 537.

---

DOI: 10.1007/s10973-007-8347-6